CrossMark

ORIGINAL PAPER

Spreading and Deposit Characteristics of a Rapid Dry Granular Avalanche Across 3D Topography: Experimental Study

Yu-Feng Wang[1,2] · Qiang Xu[2] · Qian-Gong Cheng[1,3,4] · Yan Li[1] · Zhong-Xu Luo[1]

Abstract Aiming to understand the propagation and deposit behaviours of a granular avalanche along a 3D complex basal terrain, a new 3D experimental platform in 1/400 scale was developed according to the natural terrain of the Xiejiadianzi rock avalanche, with a series of laboratory experiments being conducted. Through the conduction of these tests, parameters, including the morphological evolution of sliding mass, run-outs and velocities of surficial particles, thickness contour and centre of final deposit, equivalent frictional coefficient, and energy dissipation, are documented and analysed, with the geomorphic control effect, material grain size effect, drop angle effect, and drop distance effect on rock avalanche mobility being discussed primarily. From the study, some interesting conclusions for a better understanding of rock avalanche along a 3D complex basal topography are reached. (1) For the granular avalanche tested in this study, great differences between the evolutions of the debris along the right and left branch valleys were observed, with an obvious geomorphic control effect on avalanche mobility presented. In addition, some other interesting features, including groove-like trough and superelevation, were also observed under the control of the topographic interferences. (2) The equivalent frictional coefficients of the granular avalanches tested here range from 0.48 to 0.57, which is lower than that reached with a set-up composed of an inclined chute and horizontal plate and higher than that reached using a set-up composed of only an inclined chute. And the higher the drop angle and fine particle content, the higher the equivalent frictional coefficient. The effect of drop distance on avalanche mobility is minor. (3) For a granular avalanche, momentum transfer plays an important role in the motion of mass, which can accelerate the mobility of the front part greatly through delivering the kinetic energy of the rear part to the front.

Keywords Rock avalanche · Granular flow · 3D physical modelling · Complex topography · Mechanical energy dissipation · Momentum transfer

✉ Qian-Gong Cheng
chengqiangong@home.swjtu.edu.cn

Yu-Feng Wang
wangyufeng1987118@126.com

[1] Department of Geological Engineering, Southwest Jiaotong University, Chengdu 610031, Sichuan, China

[2] State Key Laboratory of Geohazard Prevention and Geoenvironment Protection, Chengdu University of Technology, Chengdu 610059, Sichuan, China

[3] Key Laboratory of High-Speed Railway Engineering, Ministry of Education, Chengdu 610031, Sichuan, China

[4] State-Province Joint Engineering Laboratory of Spatial Information Technology of High-Speed Rail Safety, Chengdu 610031, Sichuan, China

1 Background

Rock avalanche, as a natural phenomenon with devastating capacity in mountainous regions, is one typical example of dense granular flows, which usually presents some puzzling characteristics, such as huge volume, extremely high velocity, long travel distance, and abnormally high mobility (Heim 1932; Hadley 1978; Evans 1989; Cruden and Lu 1992; Legros 2002; Boultbee et al. 2006; Keefer and Larsen 2007; Cox and Allen 2009; Wang et al. 2009; Deline et al. 2011; Yin et al. 2011; Ostermann et al. 2012; Xu et al. 2012; Pudasaini and Miller 2013; Zhang and Yin 2013; Wang et al. 2013). Significant efforts have been

channelled towards proposing appropriate hypotheses for the rock avalanche physical motion on complex topographies, such as air or vapour lubrication (Kent 1966; Shreve 1968; Habib 1975), mechanical fluidization (Bagnold 1954; Davies 1982), acoustic fluidization (Melosh 1986), riding on basal pressure waves (Kobayashi 1994), fragmentation spreading (Davies et al. 1999), and the random kinetic energy model (Preuth et al. 2010). However, none has so far gained universal acceptance, and a lively discussion continues on this subject.

Experimentation, as an effective measure in understanding the transport mechanisms of granular flows, has been widely used in the study of rock avalanche mobility due to its advantages in phenomenological studies and the assessment of relevant physical parameters to improve the run-out prediction as well as for numerical models validation, especially in recent years (Hutter and Koch 1991; Okura et al. 2000; Félix and Thomas 2004; Pudasaini et al. 2005; Friedmann et al. 2006; Manzella and Labiouse 2008, 2009, 2013; Shea and Vries 2008; Cagnoli and Romano 2010, 2012; Mancarella and Hungr 2010; Iverson et al. 2010a, b; Mangeney et al. 2010; Yang et al. 2011; Dufresne 2012; Johnson et al. 2012; Kokusho and Hiraga 2012; Jiang and Towhata 2013; George and Iverson 2014; Kokelaar et al. 2014; Okada and Uchida 2014; Paguican et al. 2014; Bryant et al. 2015a, b; Bartali et al. 2015; Choi et al. 2015; Longchamp et al. 2015; Turnbull et al. 2015). Lineal straight or curved chutes with or without sidewise confinement are the most favoured equipment in these experimental studies. With the help of PIV, Pudasaini et al. (2005) analysed the variation in the surface velocity in dry granular avalanches and the distribution of the depth of the final deposits. Using a chute consisting of an incline and horizontal board without lateral confinement, Manzella and Labiouse (2008, 2009, 2013) observed the front velocity of the mass and the run-out, deposit morphology and thickness of the final deposit, and analysed the roles of some parameters in the granular avalanche mobility. Cagnoli and Romano (2010, 2012) studied the effects of grain size and volume on the mobility of dry granular flows and then confirmed the experimental conclusions with a 3D numerical simulation (Cagnoli and Piersanti 2015). Based on the deposit characteristics of the Xiejiadianzi rock avalanche, Yang et al. (2011) designed a series of experiments with a large flume to quantify the roles of factors affecting the granular avalanche motion, including the mass volume and initial arrangement, releasing form, particle shape and diameter, and bottom roughness. Bryant et al. (2015a, b) and Bartali et al. (2015) observed the grain-scale interaction of dry granular flows in a large-scale flume and analysed the kinematic and dynamic data of the entire granular flows, which provide an advantage for the study of granular avalanche motion. Many other studies on granular avalanche dynamics were also conducted with the equipment of chutes at laboratory scale, such as the role of the substrate entrainment (Mangeney et al. 2010; Dufresne 2012), and the formation mechanisms of levees, hummocks, and ridges (Shea and Vries 2008; Dufresne and Davies 2009; Johnson et al. 2012; Kokelaar et al. 2014; Paguican et al. 2014).

In spite of the many studies, experiments on the flow of granular avalanches down a true 3D complex basal topography are very limited in the literatures. Considering the geomorphic control effect, Iverson et al. (2004) performed bench-top experiments involving avalanches of dry sand across irregular basal topography that mimicked the complexity of natural terrain and mapped the three-dimensional morphology of the rapidly moving avalanches by laser-assisted cartography. McDougall and Hungr (2004), Pudasaini et al. (2008), and Scheidl et al. (2015) designed curved and twisted flumes to study the travel and deposit features of granular avalanches. However, how a rock avalanche propagates across a natural 3D complex basal topography, how the run-out or reach angle is affected by complex topographic conditions, and how rock avalanche deposits along a natural 3D travelling path are still poorly understood. As we all know, rock avalanches usually occur in high mountainous regions with complex morphologies displayed, such as undulated or twisted sections. Through a graphical and statistical analysis of 40 rock avalanches, Nicoletti and Sorriso-Valvo (1991) found that the display of the local morphologies of rock avalanches plays important roles in rock avalanche mobility with obvious geomorphic control effect presented. Iverson et al. (2004) also pointed out that testing the travel and deposit behaviour of granular avalanches that move across 3D topographic surfaces is a critical step towards understanding their physical motion on complex topographies of the Earth and other planets. Therefore, to learn the propagation and deposit behaviours of a granular avalanche along a natural 3D complex basal terrain and discuss the roles of material grain size, drop angle, and drop distance on rock avalanche mobility under a 3D complex geomorphology condition, a 3D physical model, mimicking the complexity of the natural terrain of the Xiejiadianzi rock avalanche, is built here and a series of tests are conducted. This study also hopes to provide powerful references for the 3D numerical simulation research on rock avalanches.

Aiming to our purpose, the design of the novel laboratory experiment is described firstly. Then, the propagation and deposit features of one granular avalanche are presented in detail, with the variations in its run-out and velocity being quantitatively documented. And a comprehensive analysis of the rock avalanche mobility under the roles of material grain size, drop angle, and drop distance is conducted with energy exchange induced by momentum

transfer in avalanche motion being analysed, quantitatively. Based on the analysis of the experimental results, a detailed comparison between the Xiejiadianzi rock avalanche and the test results is made. Finally, the geomorphic control effect, grain size effect, drop angle effect, and drop distance effect on granular avalanche mobility are discussed.

2 Methods

2.1 Scaling Design

Scaling is a critical issue in the design of laboratory experiments intended to shed light on geophysical phenomena. And some researchers have conducted the work of scaling design in their experimental studies on rock avalanches (Pouliquen 1999; Iverson et al. 2004; Cagnoli and Romano 2010; Dufresne 2012). However, due to the large number of variables acting on rock avalanches and their complexities, it is hard to realize their natural motion at laboratory scale and some rationale simplifications usually are included in their scaling design processes (Dufresne 2012). So, instead of reproducing a natural rock avalanche at the laboratory scale, the aim of the laboratory

experiments becomes to strip away confounding influences that are prevalent in nature and thereby reveal phenomenology that is difficult to observe or measure in the field (Shea and Vries 2008; Iverson 2015). For the macroscopic dimensional analysis of avalanches without fluid, Iverson (2015) proposed a general functional relationship between the evolving downslope velocity and the macroscopic referenced variables in the following dimensionless form

$$\frac{\boldsymbol{u}}{\sqrt{\mathbf{g}L}} = f\left(\frac{H}{L}, \frac{\sigma}{\rho \mathbf{g} H}, \frac{t}{\sqrt{\frac{L}{\mathbf{g}}}}, \varphi, \theta\right), \tag{1}$$

where f represents an unknown function; $\boldsymbol{u}$ is the evolving downslope velocity of the mass; $\mathbf{g}$ is the gravitational acceleration; ρ, L, and H are the bulk density, length, and thickness of the moving mass, respectively; φ is the basal Coulomb friction angle; θ is the slope angle; and t is time.

The Xiejiadianzi rock avalanche is a typical lengthened stalled rock avalanche in plan (Dunning et al. 2005) triggered by the Wenchuan earthquake, which is located on the right bank of the Baishui River, Pengzhou City (Fig. 1) (Wang et al. 2015). The slope angle of its source area ranges from 30° to 45°. As a coseismic rock avalanche, its volume detached from the source area is about
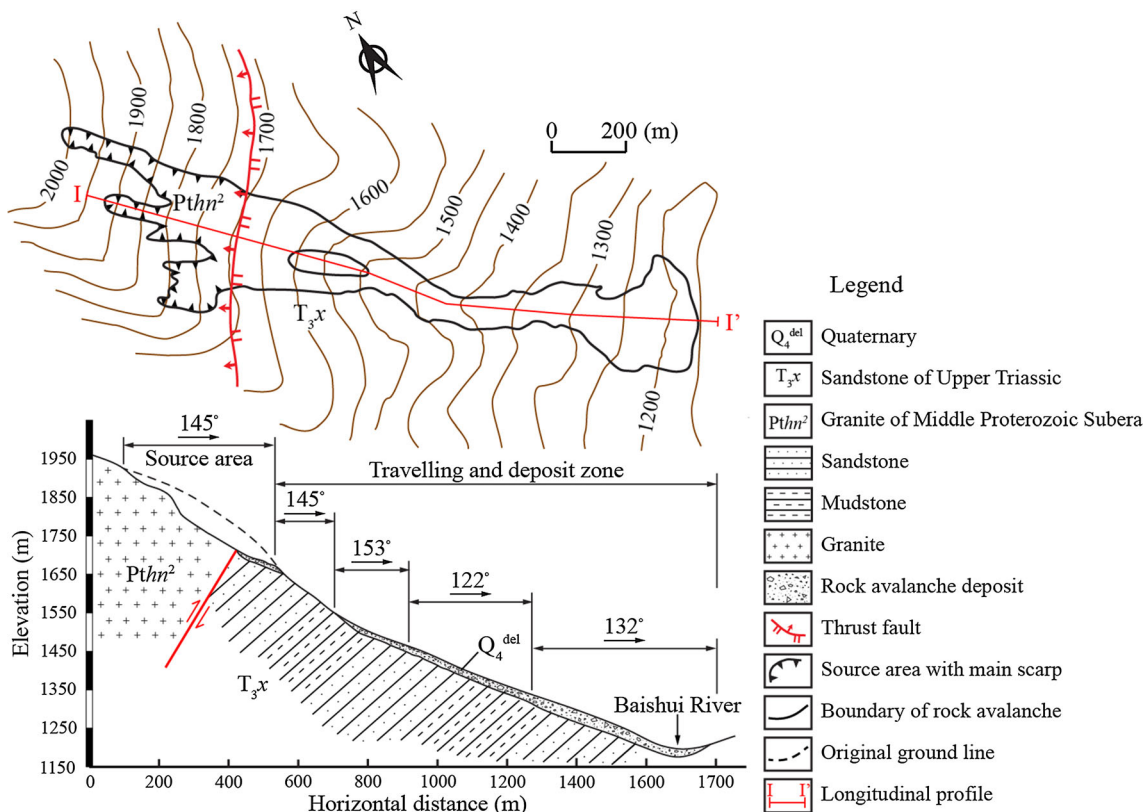

Fig. 1 Plan view and longitudinal profile of the Xiejiadianzi rock avalanche

Table 1 Summary of the key variables used in the dimensional analysis

Item	Symbol	Dimension	π	Scaling ratio
Length	L	[L]	Controlling parameter	1:400
Volume	V	[L^3]	$\pi_V = L^3$	1:400^3
Gravity acceleration	g	[LT^{-2}]	Controlling parameter	1:1
Slop angle	θ	[M^{0}L^{0}T^0]	1	1:1
Bulk density of moving mass	ρ	[ML^{-3}]	Controlling parameter	1:1
Particle density	ρ_s	[ML^{-3}]	$\pi_{\rho_s} = \rho$	1:1
Basal friction angle	φ	[M^{0}L^{0}T^0]	1	1:1
Time	t	[T]	$\pi_t = L^{0.5}g^{-0.5}$	1:20
Velocity	u	[LT^{-1}]	$\pi_u = L^{0.5}g^{0.5}$	1:20

0.5×10^6 m^3 with a 1.7 km run-out and 700 m vertical drop. And due to the fragmentation and intensive entrainment of the sliding mass in motion, its accumulated volume reached 1.1×10^6 m^3 (Wang et al. 2013). As mentioned above, this study aims only to learn the propagation and deposit characteristics of a granular avalanche along a natural 3D basal terrain, no attempt is made to reproducing the natural phenomena of the Xiejiadianzi rock avalanche. Hence, a simplified scale design was conducted based on Eq. (1), and a laboratory scale of 1:400 was selected here for the design of the experimental set-up. The scaling ratios of the key variables used in this dimensional analysis are listed in Table 1.

2.2 Experimental Set-up

Figure 2b is an overview of the experimental set-up designed at the 1:400 scale, with its dimensions being approximately 4.8 m long, 1.6 m high, and 1.0 m wide. Longitudinally, the experimental set-up is composed of two parts, i.e. the source area and travelling path (Fig. 2b), which are joined by a hinge to keep the changeability of the drop angle of the material released from the source area (Fig. 3). For the convenience of the control of the failure mode of the released material, the source area of the experimental set-up is simplified to an inclined panel with a box 53 cm long, 42 cm wide, and 15 cm high installed to contain material (Figs. 2b, 3). The travelling path of the experimental set-up is made of smooth plexiglass plate, with complex topographic interferences being manufactured based on the topographic map of the travelling path of the Xiejiadianzi rock avalanche (Fig. 2a) with a small divide, convex banks, bend points, and lateral small platform displayed (Fig. 2b). On the surface of this section, gridlines at 2 cm interval were marked to realize the reading of the debris run-out (Fig. 2b).

Each test was viewed by four digital video cameras with three (i.e. Cameras 1–3) positioned above the travelling path and one (i.e. Camera 4) placed in front of the experimental set-up (Fig. 3). Cameras 1–3, instead of

taking photographs, were used to record videos of the propagation of the granular avalanche with high definition 1080, which allows us to obtain more data on the run-out and velocity variations in the granular avalanche. To assure the accuracy of the avalanche run-out measured manually using the videos recorded by Cameras 1–3, we divided the travelling path into three sections for monitoring, with Cameras 1–3 being positioned perpendicular to the centre point of each section as exhibited in Fig. 3. In addition, a three-dimensional laser scanner was employed to acquire the thickness contour of the final deposit of the granular avalanche in each test, used to realize the calculation of the final deposited mass centre. To avoid the error induced by laser refraction on plexiglass during the scanning, a very thin purple layer was painted on the surface of the travelling path (Fig. 2b) with a low roughness generated.

For the capture of the run-out and velocity of the granular avalanche, four trace particles, labelled with Nos. 1–4, were placed on the surface of each sample prior to testing (Fig. 4). Here, the run-out is defined as the inclined travel distances of these trace particles along the base of the model away from the leading edge of the source area. And the velocity refers to the velocities of these trace particles calculated using their run-outs and the video image sequence. Considering the asynchronism of the beginning time of Cameras 1–3, four autosynchronous stopwatch timers were installed along the travelling path to record the travel time of the mass (Fig. 2b).

Through the combination of these detection measures, abundant experimental results on the rock avalanche evolution along a natural 3D basal terrain were obtained, including the avalanche propagation forms, surficial velocities of different particles, thickness contour of the final deposit, and position of the centre of mass. These data allow us to compute the travel angle of the centre of mass, analyse the energy dissipation of the granular avalanche, and discuss the role of momentum transfer during avalanche motion, which are advantageous for the study of rock avalanche dynamics.
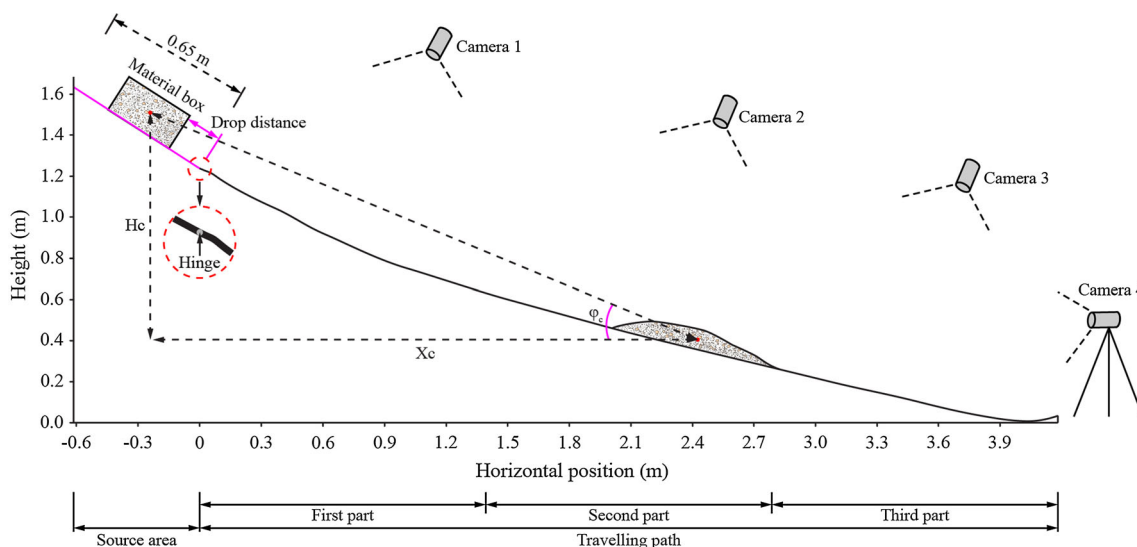
Fig. 2 View of the 3D equipment platform and the topographical map of the travelling path
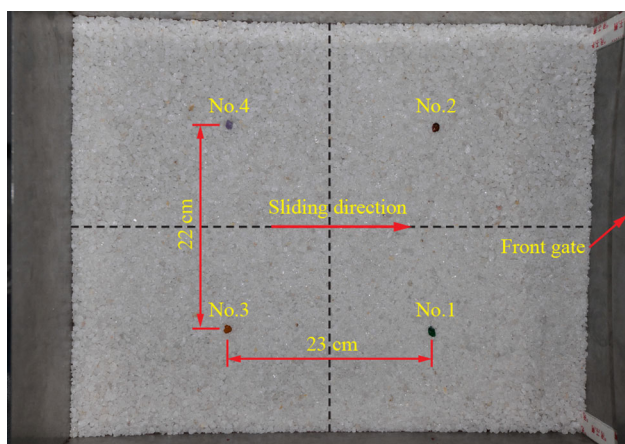

(a)   **(b)**
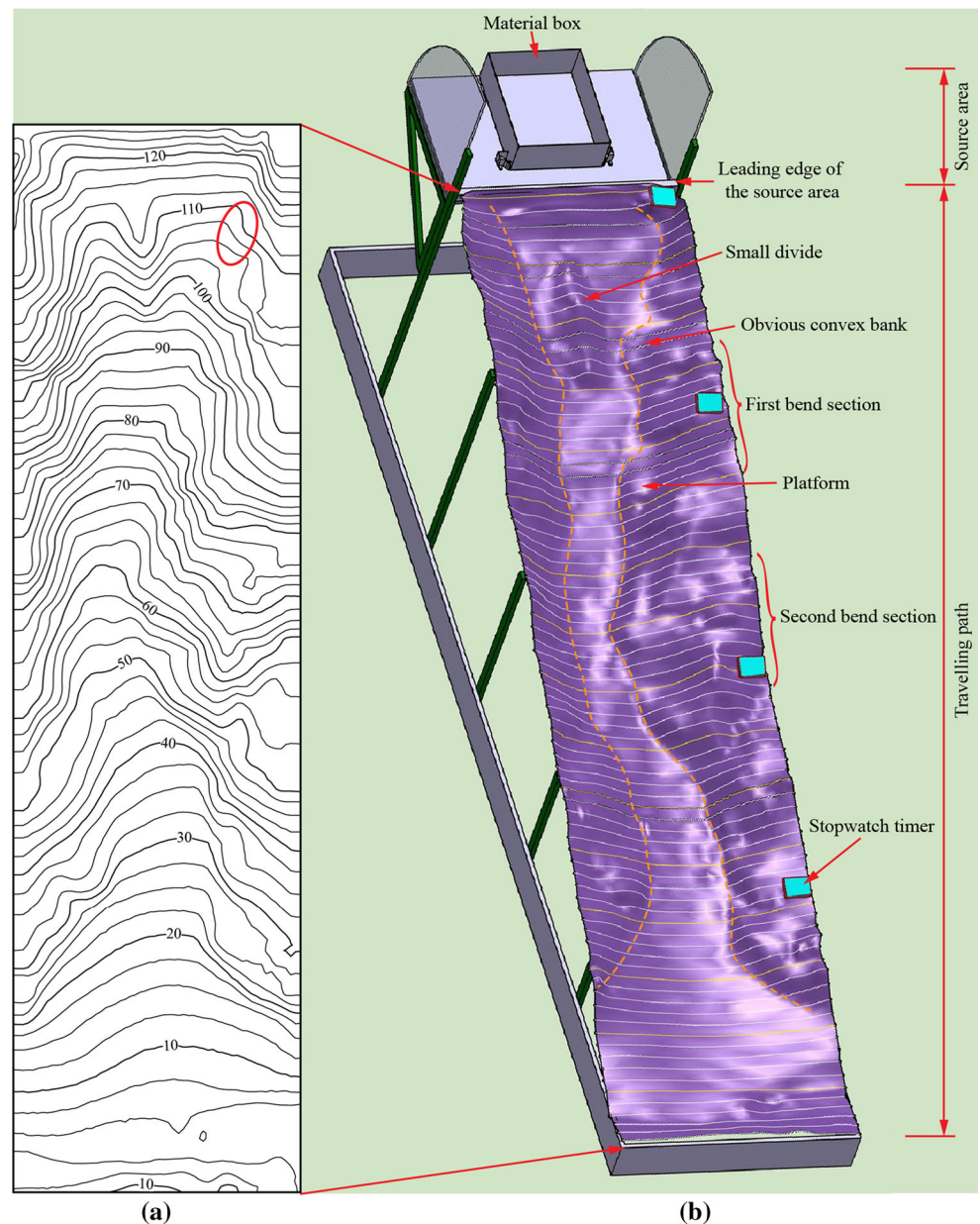
2.3 Selection of Test Conditions

As previously mentioned, despite the difficulty in reproducing a natural rock avalanche at laboratory scale, simplified physical models are still useful in investigating the propagation and deposit features of a granular avalanche, especially in the study of the roles of parameters of interest (Manzella and Labiouse 2008, 2009, 2013; Cagnoli and Romano 2010, 2012; Mangeney et al. 2010; Yang et al. 2011; Bryant et al. 2015a, b; Bartali et al. 2015). Therefore, based on the parameters of the Xiejiadianzi rock avalanche, the following factors are considered in this study to evaluate their roles on the granular avalanche mobility along a natural 3D basal terrain.

1. Nature of released material: angular-shaped quartz grain;
2. Material volume: 9.7×10^{-3} m^3 (17.6 kg), corresponding to 0.62×10^6 m^3 in natural scale, which is a little higher than the detached volume of the Xiejiadianzi rock avalanche, 0.5×10^6 m^3;
3. Material grain size: 0.1–7 and 2–7 mm; details are introduced as follows:
4. Drop angle: 25°, 30°, 35°, and 40°;
5. Drop distance: 30, 34, and 38 cm. Here, drop distance points to the distance between the front gate of the material box and the leading edge of the source area as shown in Fig. 3, used to simulate the short accelerated motion of the rock avalanche before ejection from the
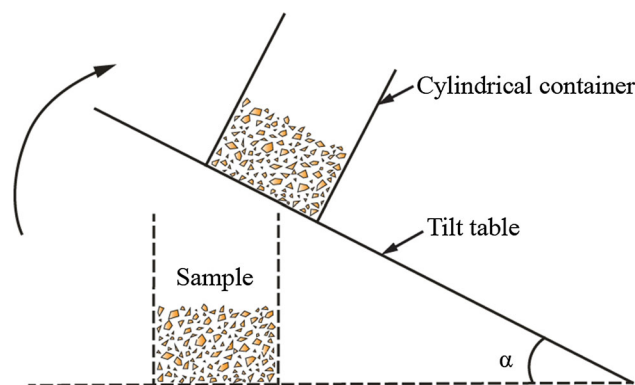
Fig. 3 Schematic illustration of the 3D equipment platform and arrangement of cameras

Fig. 4 Plan view of the arrangement of the trace particles in material box

Fig. 5 Schematic illustration of the tilt table apparatus used to test the friction coefficient of material

leading edge of the source area (i.e. the toe of surface of rupture). The selection of these values is based on the length of the source area and the travelling speed of the Xiejiadianzi rock avalanche calculated by Dai et al. (2011).

The reasons why selecting angular-shaped quartz grains as the releasing material are as follows: (1) The particle density of the quartz grains is 2.65 g/cm^3, which is close to that (2.85 g/cm^3) of the Xiejiadianzi rock avalanche deposits, meeting the scaling ratio listed in Table 1. (2) These quartz grains were obtained by crushing rock blocks and sieving the fragments with their original fractured angular morphologies well, which are similar to the angular morphologies of rock avalanche debris. (3) Through a series of quasi-static measurements using a tilt

table apparatus (Fig. 5), we obtained that the averaged basal frictional coefficients of the quartz grains and the Xiejiadianzi rock avalanche debris are close, with values of 0.486 and 0.438, respectively (Table 2), which meets the scaling ratio listed in Table 1.

In addition, during our field investigation, a vertical grain size distribution of the Xiejiadianzi rock avalanche deposit was conducted by combining an area-by-area technique and a sieve analysis, revealing that the grain size of the deposit generally ranges from 5 to 350 mm with obvious inverse grading displayed (Wang et al. 2012). On the surface of the deposit, large blocks of 0.35–1 m diameter are common (Fig. 6a), with some even reaching 2–3 m in diameter (Fig. 6b, c). Therefore, based on the actual grain size distribution of the Xiejiadianzi avalanche deposit and considering the occurrence of particle fragmentation during avalanche motion (Davies et al.

Table 2 Frictional parameters of the prototype and model samples

	First series			Second series		
	Mass of samples (kg)			Mass of samples (kg)		
	1.5	2	2.5	1.5	2	2.5
Prototype						
Normal stress (Pa)	602.6	801.9	1003.4	602.0	801.9	1004.4
Shear stress (Pa)	268.1	353.4	430.3	270.6	353.4	426.9
Friction coefficient	0.45	0.44	0.43	0.45	0.44	0.43
Basal friction angle (°)	22°			21.22°		
Cohesion (Pa)	25.92			38.43		
Averaged friction coefficient	0.44					
Model						
Normal stress (Pa)	595.2	792. 7	992.0	595.5	792. 7	991.4
Shear stress (Pa)	297.1	385.4	467.9	295. 9	385.4	469.6
Friction coefficient	0.50	0.49	0.47	0.5	0.49	0.4794
Basal friction angle (°)	23.28°			23.67°		
Cohesion (Pa)	42.01			35.62		
Averaged friction coefficient	0.49					

Fig. 6 Display of coarse-grained material deposited on the surface of the Xiejiadianzi rock avalanche
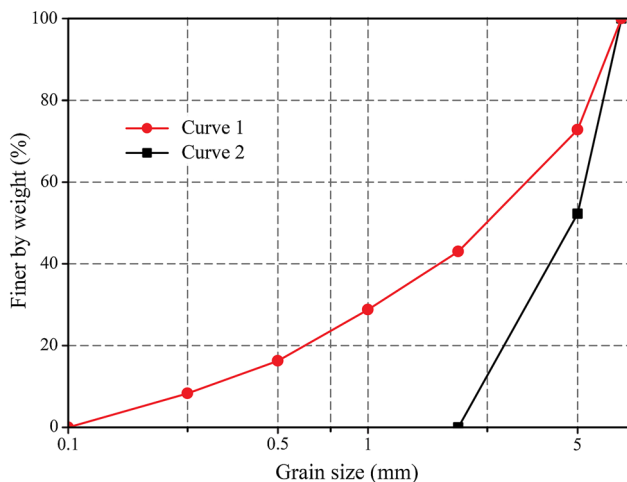
Fig. 7 Grain size distributions of the materials used in this study

1999), materials of 0.1–7 mm diameter (Curve 1 in Fig. 7) (corresponding to the grain size ranging from 5 to 350 mm in natural setting) and only composed of coarse particles in 2–7 mm (Curve 2 in Fig. 7) were used in this study to analyse the grain size effect on the rock avalanche mobility along the 3D basal terrain.

Detailed information on the test conditions is given in Table 3.

3 Results and Analysis

### 3.1 Observations of Avalanche Behaviour

Taking the example of the test No. III, an introduction of the propagation and deposit features of the granular avalanche along the 3D basal terrain is depicted. Figure 8 shows the whole propagation process of the granular avalanche, photographed by Camera 4. And Fig. 9 is some close-up views of the spreading details of the granular avalanche videoed by Cameras 1–3, with the variations in the run-outs and velocities of the trace particles being depicted in Figs. 10 and 11, respectively. Here, the leading

Table 3 Test conditions and corresponding tested data of mass centre

Test no.	Material	Test conditions					Tested data of mass centre			Bulk energy dissipation (J/m)
		Mass (kg)	Basal friction	Diameter (mm)	Drop angle (°)	Drop distance (cm)	X_c (cm)	H_c (cm)	μ_c	
I	Quartz gravel	17.6	Nearly smooth	2–7	25	30	124.1	59.7	0.481	74.7
II					30	30	137.4	68.8	0.501	77.3
III					35	30	147.3	77.4	0.526	80.2
IV					40	30	144.2	81.7	0.566	85.0
V					35	34	154.2	81.0	0.525	80.7
VI					35	38	169.4	88.8	0.524	80.1
VII				0.1–7	35	38	142.1	78.4	0.551	83.3
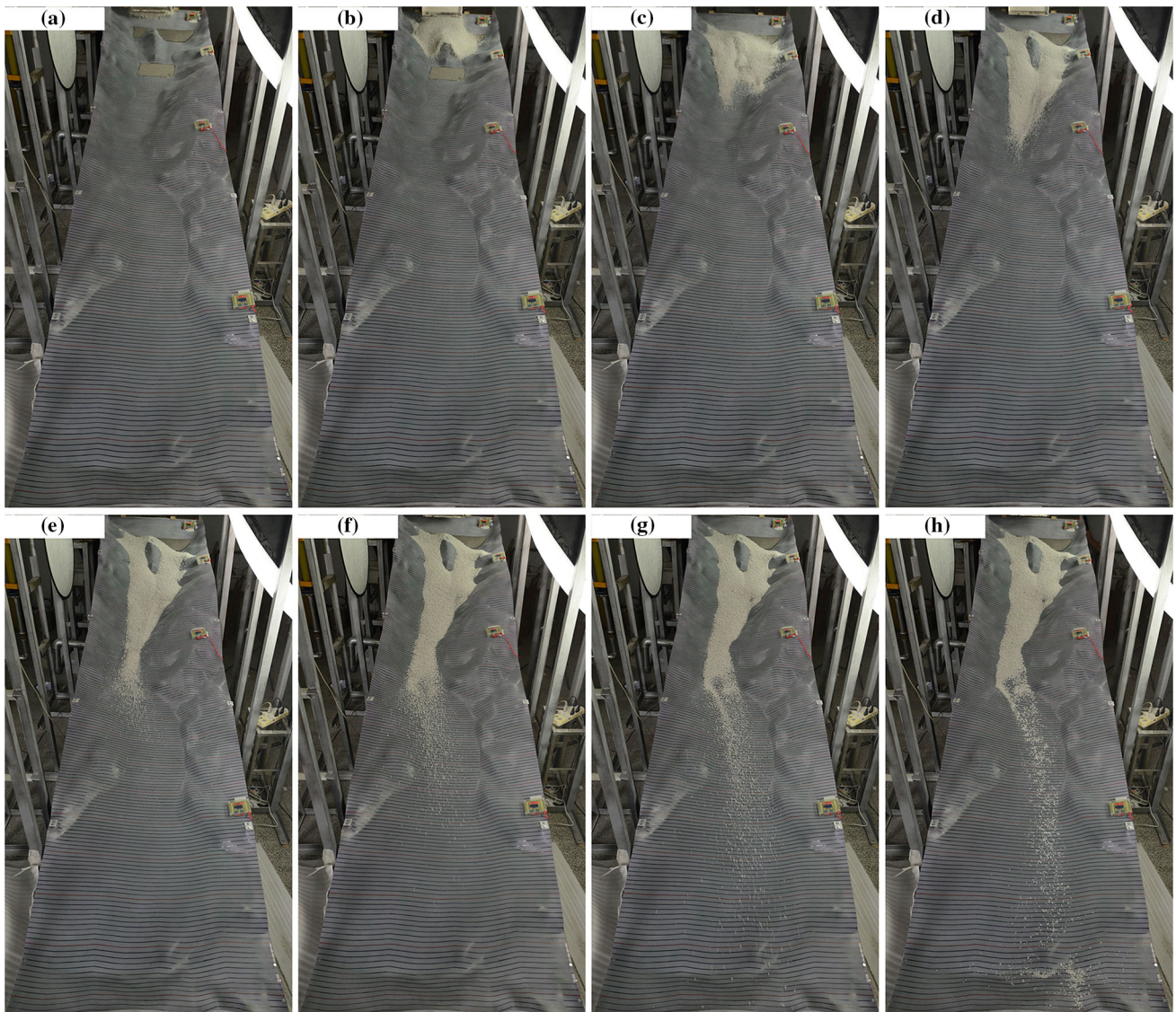
Fig. 8 Snapshots of the propagation of the granular avalanche of the test No. III. **a** t = 0.08 s, **b** t = 0.29 s, **c** t = 0.54 s, **d** t = 0.79 s, **e** t = 1.05 s, **f** t = 1.30 s, **g** t = 1.55 s, **e** t = 4.08 s
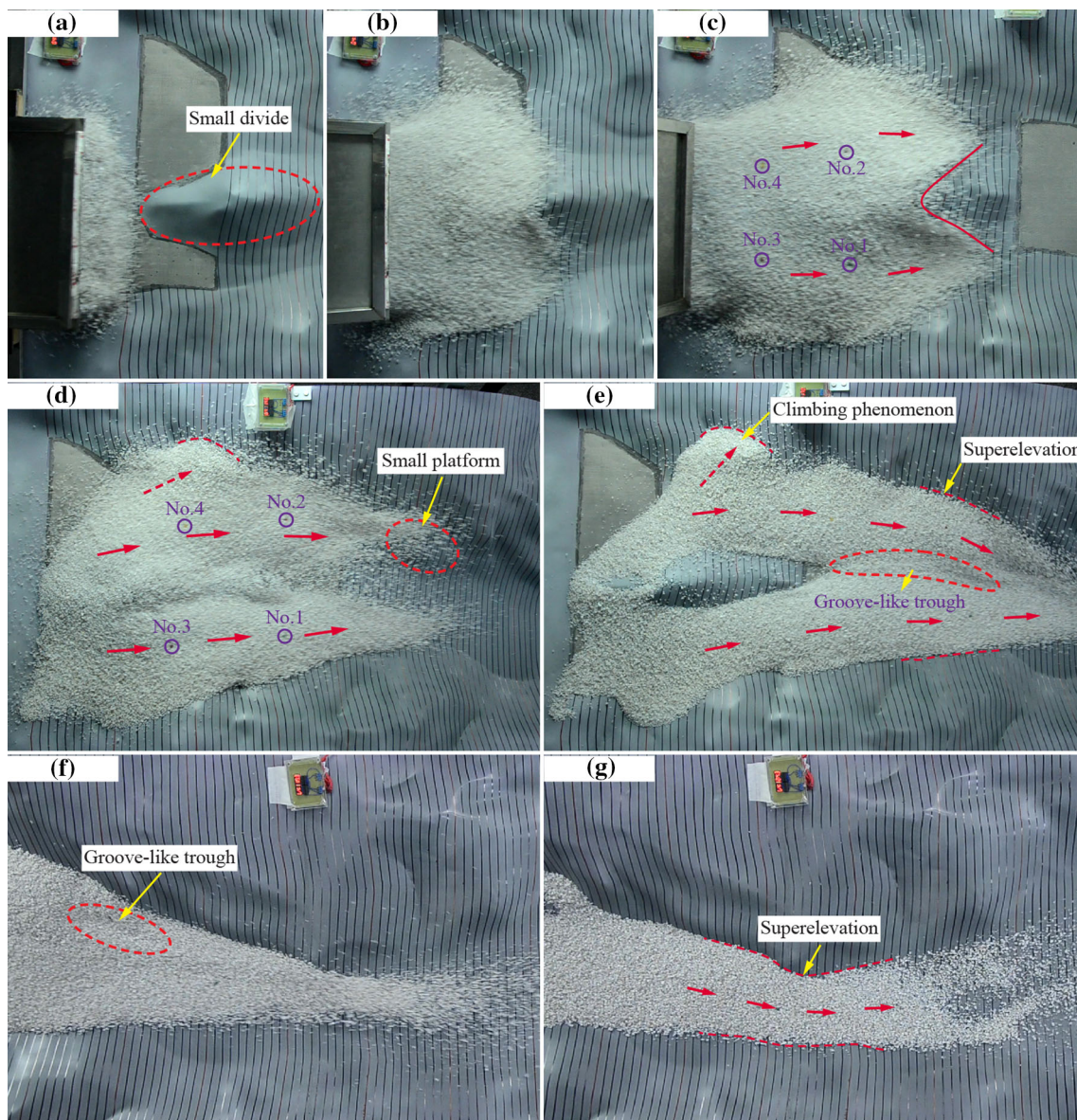
Fig. 9 Close-up views of the spreading details of the granular avalanche of the test No. III. **a** t = 0.09 s, **b** t = 0.21 s, **c** t = 0.30 s, **d** t = 0.54 s, **e** t = 0.80 s, **f** t = 1.03 s, **g** t = 1.53 s

edge of the source area is the starting point of the mass run-out (Figs. 2b, 3), and the time when the mass is released from the source area is the start time of recording. Figure 12 is an illustration of some close-up views of the final deposit of the granular avalanche.

From the propagation of the granular avalanche shown in Fig. 8, it can be observed that the total travelling time of the mass is approximately 4.1 s. Within this period, the travelling duration of the main mass is only approximately 1.5 s, with the rest being cost in the bouncing process of these particles travelling along the lower part of the path. Under the control of the basal topography, the propagation of the granular avalanche can be divided into three stages,

as inspected in Fig. 9, i.e. the initial failure stage (Fig. 9a, b), the diverted flow stage (Fig. 9c, d), and the movement stage after convergence (Fig. 9e, f). Corresponding to the motion of the avalanche, most of the debris finally deposited in the upper part of the travelling path with limited particles sporadically accumulating in the lower part (Fig. 8h). Similar features were also observed in other tests, with the mass mainly deposited in the upper part of the travelling path, as exhibited in Fig. 20 in "Appendix" section.

During the initial failure stage, the mass first moved as a whole (Fig. 9a), with lateral spreading exhibited as it continued to move (Fig. 9b). It was then diverted into two
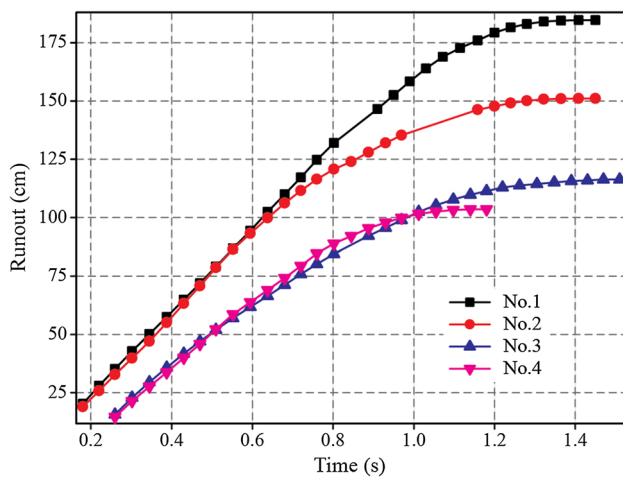
Fig. 10 Run-out variations in the trace particles with time
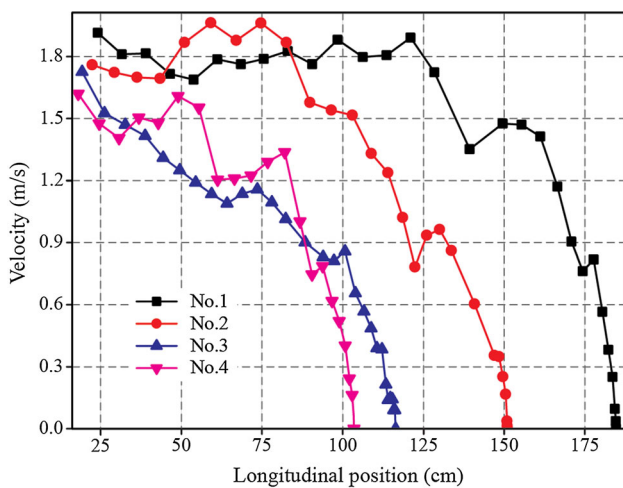
Fig. 11 Velocity variations in the trace particles with longitudinal position

parts due to the obstruction of the small divide near the source area and continued to move along both branch gullies (Fig. 9b, c). Accompanied with the divergence of the avalanche, the No. 1 and No. 3 trace particles fell into the right branch gully and the No. 2 and No. 4 trace particles fell into the left branch gully, as revealed in Fig. 9d.

In the subsequent diverted flow stage with the run-out ranging from 23 to 90 cm, some important propagation behaviours of the granular avalanche are inspected in Figs. 8, 9, 10, and 11. The most conspicuous phenomenon is the different spreading forms of the avalanche in the right and left branch gullies. For example, due to the control of the topography along the left bank of the left branch gully (labelled with the red ellipsoid in Fig. 2a), a climbing phenomenon occurred as exhibited in Fig. 9d, e. In addition to this, a great velocity variation was observed for the debris in the left branch valley as

revealed by the No. 2 trace particle in Fig. 11. In the range of 40–60 cm, the velocity of the No. 2 trace particle displayed an obvious increase, with its value increasing from 1.69 to 1.96 m/s. After a short steady motion, it began to decrease rapidly from 1.96 m/s (Fig. 11) due to the appearance of the convex terrain at a distance of 70 cm along the left bank of the left branch gully (Fig. 2). Greatly different from the velocity variation in the No. 2 trace particle, the velocity of the No. 1 trace particle in the right branch valley presented a relatively stable trend with only small fluctuations (Fig. 11). This great velocity difference between the No. 1 and No. 2 trace particles in this stage powerfully indicates the key role of geomorphic control (i.e. local lateral confinement) on the avalanche mobility.

Accompanying the convergence of the debris from both branch valleys, a superelevation phenomenon was observed as shown in Fig. 9e due to the inhabitation of the terrain along the left bank at a distance of 115.0 cm, where the first bend terrain appeared (Fig. 2). And a negative flowing relief (groove-like trough) presented with the convergence of the debris (Fig. 9e). At the same time, the velocity of the main sliding mass began to decrease as revealed in Fig. 11. When the mass reached the position where a small platform distributed (Figs. 2, 9d), a bouncing process occurred under the control of the platform with some particles separating from the main sliding mass (Fig. 9e) and converging latterly. With the convergence, a groove-like trough morphology appeared on the surface of the sliding mass (Fig. 9f) and ultimately deposited (Fig. 12b). As the mass continued to move, a centrifugal movement presented again from 165.0 to 220.0 cm (Fig. 9g), where the second bend terrain appeared (Fig. 2). When the mass reached over 250.0 cm away from the source area, a lateral spreading and bouncing phenomenon of particles occurred as the abrupt opening of the travelling path and the rapid decrease in the sliding mass volume (Fig. 8f–h). Finally, a climbing phenomenon was observed on the opposite slope of the travelling path (Fig. 12c).

In addition to the features mentioned above, there are both other conspicuous behaviours being revealed during the motion of the granular avalanche. One is the great variation in the avalanche width in both time and space under the control of the topography. The other is the time lag effect revealed in the variations in the trace particle velocities corresponding to topography changes. For example, under the obstruction of the convex terrain situated at a distance of 70 cm along the left bank of the left branch gully, the velocity reduction in the No. 2 particle appeared when it reached 82.5 cm (Fig. 11), which is obviously farther than the position where the convex terrain extended.
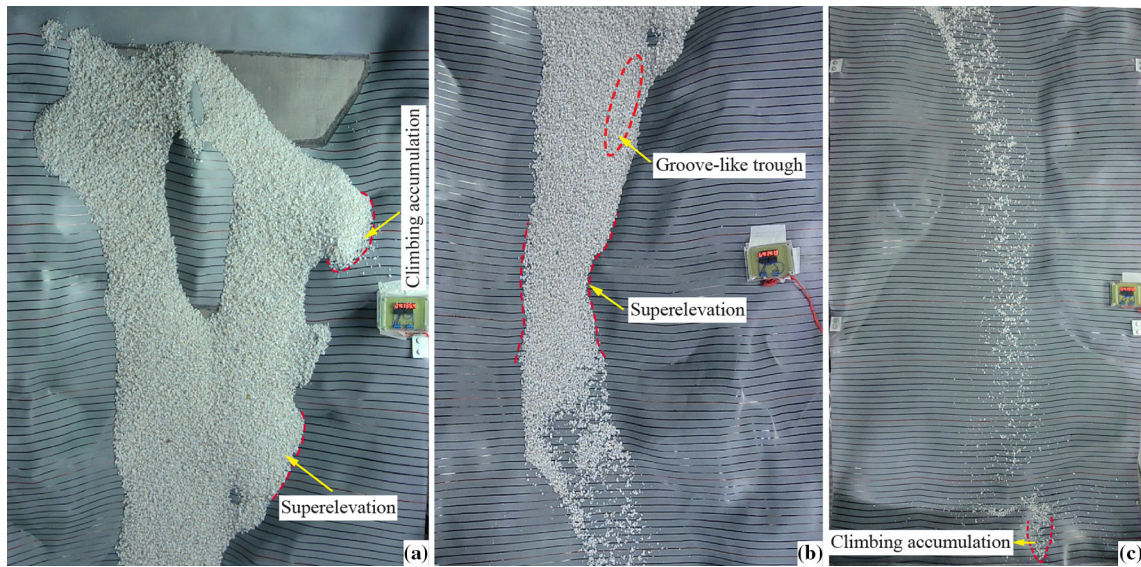
Fig. 12 Close-up views of the final deposit details of the granular avalanche of the test No. III
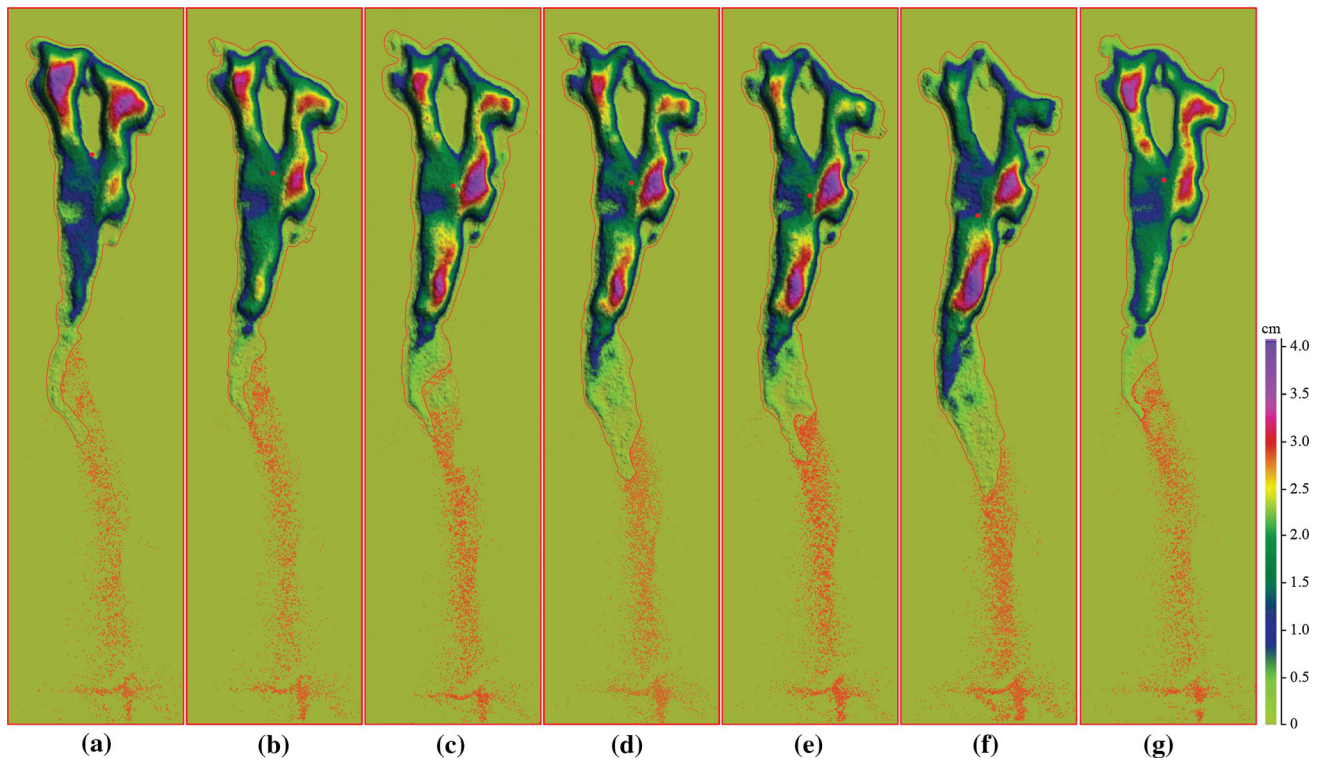
Fig. 13 Deposition thickness contours of the granular avalanches of the test Nos. I–VII (the *red solid circle* is the position of the centre of deposited mass). **a** Test No. I, **b** test No. II, **c** test No. III, **d** test No. IV, **e** test No. V, **f** test No. VI, **g** test No. VII (colour figure online)

3.2 Roles of the Factors on Granular Avalanche Mobility

As aforementioned, a three-dimensional laser scanner was used in this study to acquire the height information of the final deposit in each test with their thickness contours being reached as shown in Fig. 13. Because the particles in the lower part of the travelling path were present in sporadic distributions with their deposited thickness too thin to read, red dots were used to highlight the particles in the lower part in Fig. 13. Based on the displays of the thickness contours of these avalanche final deposits, the positions of

their mass centres were calculated, which allows computing the travel angle of the centre of mass (φ_c) (Fig. 3). In the following, the equivalent frictional coefficient ($\mu_c = \tan \varphi_c$), i.e. the ratio of the vertical drop (H_c) and horizontal run-out (X_c) of the centre of mass (Fig. 3), is used for analysis. In Table 3, the data of the mass centre run-outs and corresponding equivalent frictional coefficients (μ_c) of all tests considered in this article are listed. And the positions of all tested mass centres are labelled with red solid dots in Fig. 13. In Figs. 14 and 15, the vertical drops versus horizontal run-outs of the centres of the tested masses with their equivalent frictional coefficients against the drop angle, drop distance, and material grain size are plotted, respectively.

As shown in Figs. 13a–d, 14, and 15a, the results of test Nos. I–IV with a constant drop distance and material grain size (Table 3) are presented, which provides the possibility of observing the role of the drop angle on the avalanche mobility. From Fig. 13a–d, it can be observed that when the drop angle ranges from 25° to 35°, the final deposit area
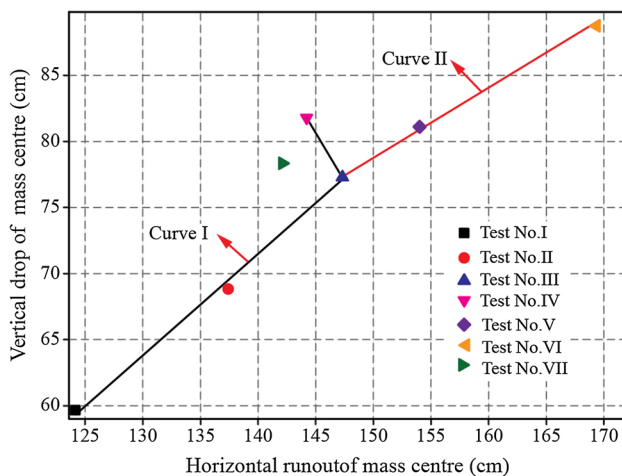
of the avalanche mass clearly moves downward with the increasing drop angle. And the equivalent frictional coefficients of the granular avalanches present a linear gentle increasing trend with the increasing drop angle (Fig. 15a). When the drop angle increases to 40° from 35°, there is almost no downward extension of the deposit scope of the avalanche mass (Fig. 13c, d). And as revealed in Fig. 13c, d and Table 3, the horizontal run-out of the mass centre in test No. IV is slightly lower than that obtained in test No. III. Corresponding to the deposit morphologies of both tests, an abrupt turning point appeared in Curve I as shown in Fig. 14. At the same time, different from the gentle linear increasing trend of the equivalent frictional coefficients of the granular avalanches obtained in test Nos. I–III, that reached in test No. IV shows a steep increase, as revealed in Fig. 15a. The results of test Nos. I–IV imply that when the value of the drop angle is lower than a threshold, a relatively gentle decrease in the mobility of the granular avalanche along a natural 3D complex terrain can be reached. However, when the drop angle is over the threshold, a higher energy dissipation rate will occur as the increasing drop angle. To further prove the reliability of the result, some parallel tests, with a drop distance and material grain size being 34 cm and 2–7 mm, respectively, were conducted (Table 5 in "Appendix" section), and the same conclusion was also reached as shown in Fig. 21 in "Appendix" section. In addition, in the laboratory study conducted by Manzella and Labiouse (2013) using a set-up composed of an inclined chute and horizontal plate, an even higher energy dissipation rate was reached, i.e. the equivalent frictional coefficient of the centre of mass increases obviously ($0.7 \rightarrow 0.8$) when the drop angle increases from 37.5° to 45°. Further investigation will be conducted in the future to explore the reason for this phenomenon.

Figures 13c, e, f, 14, and 15b give a general overview of the results of test Nos. III, V, and VI with a constant drop angle and material grain size (Table 3), providing the possibility of observing the role of the drop distance on the

Fig. 14 Plot of the vertical drops of the centres of the avalanches against their horizontal run-outs
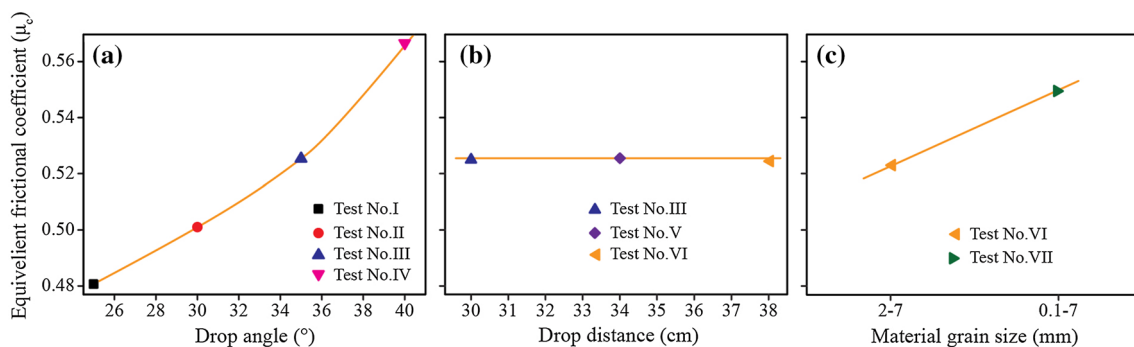

Fig. 15 Plots of the equivalent frictional coefficient against drop angle, drop distance, and material grain size

avalanche mobility. Through a contrast of the deposit morphologies of the avalanche masses presented in Fig. 13c, e, f, a relatively minor downward spreading of the deposit scope of the avalanche masses occurs with the increasing drop distance, especially for test Nos. III and V (Fig. 13c, e). Corresponding to the deposit morphologies revealed in Fig. 13c, e, f, their equivalent frictional coefficients are almost constant as shown in Fig. 15b, which indicates that the increase in the drop distance has a very minor influence on the mobility of the granular avalanche on the natural 3D complex terrain. Parallel to this study, a series of tests, with a drop angle and material grain size of 30° and 2–7 mm, respectively, were also carried out (Table 5 in "Appendix" section). A similar law was reached as exhibited in Fig. 22 in "Appendix" section, which further proves the reliability of this study.

In Figs. 13f, g, 14, and 15c, it is possible to analyse how the use of different grain size groups influences the avalanche mobility. As shown in Fig. 13f, g, the run-out of the material composed of coarse particles of 2–7 mm diameter (test No. VI in Table 3) is obviously higher than that of the material with finer particles (test No. VII in Table 3). And the value of the equivalent frictional coefficient of mass tends to increase with increasing fine particle concentration (Fig. 15c). This implies that a higher fine particle concentration can reduce the mobility of a granular avalanche along the natural 3D complex terrain. In the flume tests conducted by Kokusho and Hiraga (2012), a similar law was also observed. To explain this feature, Drake (1991) found that the existence of fine particles can induce an electrostatic effect on the motion and reduce the mobility of a granular flow. Hence, a possible reason for the difference in the avalanche mobility of test Nos. VI and VII could be the distribution of fine particles (ranging from 0.1 to 0.5 mm in diameter) in test No. VII, which induced an electrostatic effect along the basal surface of the travelling path and decreased the mobility of the avalanche.

3.3 Momentum Transfer in Granular Avalanche

Momentum transfer within a rock avalanche has been noticed more than 100 years since the study of the Elm avalanche by Heim in 1882 (Hsü 1975). In the experimental study conducted by Manzella and Labiouse (2009), a transfer of momentum was also observed between the rear approaching part and the front part of the sliding mass, which accelerated the velocity of the front part. In this study, four trace particles with different positions were placed on the surface of the granular avalanche in each test (Fig. 4), which allows the calculation of the surficial velocities of the different parts of the sliding mass (Fig. 11) and gives an opportunity to quantify the effect of momentum transfer in the avalanche motion. For the
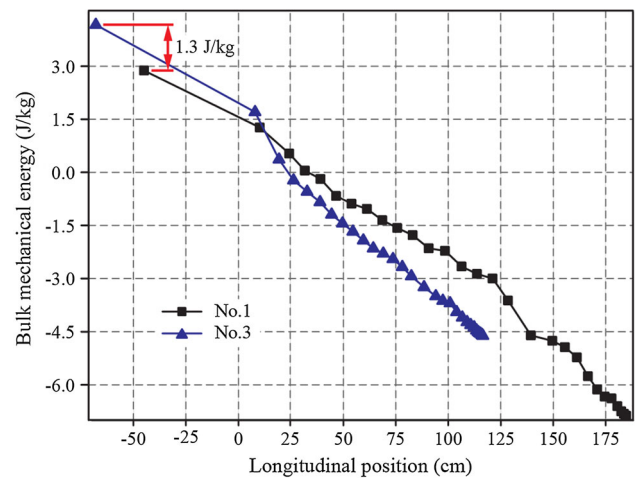
Fig. 16 Bulk mechanical energy variations in the Nos. 1–3 particles with longitudinal position of the test No. III

following analysis, the velocities of the No. 1 and No. 3 trace particles obtained in test No. III are used (Fig. 11), with their bulk mechanical energies being reached as exhibited in Fig. 16. In the part II of the appendix, the calculation of the bulk mechanical energies shown in Fig. 16 is presented. Here, the leading edge of the source area is defined as the zero potential level. And the bulk mechanical energy is defined as the mechanical energy of a unit granular mass.

In Fig. 16, the curves of the bulk mechanical energies of the No. 1 and No. 3 particles are graphed for analysis. From this figure, it can be observed that the initial bulk mechanical energy of the No. 3 particle in the rear part is higher than that of the No. 1 particle in the front part, with their difference being 1.3 J/kg. After being released from the source area, the No. 1 and No. 3 particles both fell into the right branch valley of the travelling path (Fig. 9d), with nearly overlapping trajectories presented. If we divide the mass into four parts as shown in Fig. 4 and use the four trace particles in each part to represent each part, the motion of the sliding mass travelling along the right branch valley can be represented by the movements of the No. 1 and No. 3 particles. And the momentum transfer occurred in the rear and front parts of the mass travelling along the right branch valley can be regarded as the interaction between the No. 1 and No. 3 particles. To quantify the energy exchange induced by momentum transfer during the avalanche motion, we assume that particle collision is elastic and the energy is completely dissipated by basal friction. Under this assumption and considering the complexity of the natural granular avalanche motion, we just calculated the total energy losses of the No. 1 and No. 3 particles according to their initial and final positions to calculate the energy exchange between them for particle
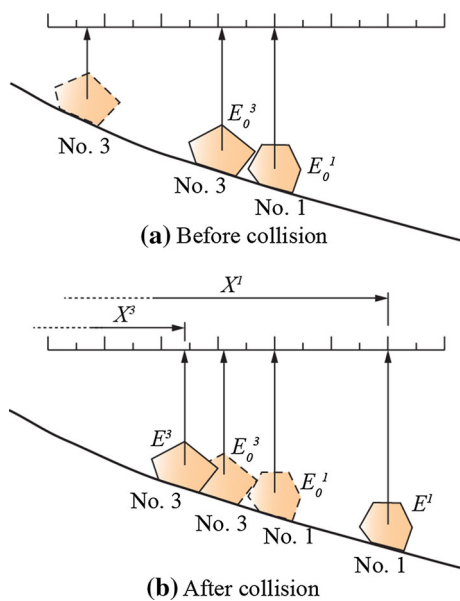
Fig. 17 Conceptual diagram of the momentum transfer process between particles

collisions. The bulk mechanical energy (E) of them can be expressed as (Fig. 17),

$$E^i = E_0^i - \Delta E_f^i - \Delta E_m^i \qquad (2)$$

where i is used to represent the number of particle; E_0^i is the initial bulk mechanical energy of particle i; and ΔE_f^i and ΔE_m^i are the bulk energy changes in particle i induced by friction and momentum transfer, respectively. Using Eq. (2), we can reach that the difference in the bulk mechanical energies between the No. 1 and No. 3 particles is

$$E^3 - E^1 = E_0^3 - E_0^1 - \left(\Delta E_f^3 - \Delta E_f^1\right) - \left(\Delta E_m^3 - \Delta E_m^1\right) \qquad (3)$$

Figure 17 is a conceptual diagram of the momentum transfer process between particles. Here, we suppose that the energy dissipation induced by friction is same for different particles with same trajectory, and the bulk frictional energy (ΔE_f^i) of particle i can be expressed as a function of the equivalent frictional coefficient (μ_c) and horizontal run-out (X^i). From Fig. 10, it can be reached that the run-outs of the No. 1 and No. 3 particles are 184.7 and 116.4 cm. Therefore, with the simplification, it can be calculated that the bulk frictional energies of the No. 1 and No. 3 particles after their motions are

$$\begin{cases} \Delta E_f^1 = \mu_c g X^1 = 0.526 \times 9.80 \text{ m/s}^2 \times 1.847 \text{ m} = 9.52 \text{ J/}kg \\ \Delta E_f^3 = \mu_c g X^3 = 0.526 \times 9.80 \text{ m/s}^2 \times 1.164 \text{ m} = 6.00 \text{ J/kg} \end{cases} \qquad (4)$$

With the above-mentioned elastic collision assumption, we can conclude that ΔE_m^1 is equal to $-\Delta E_m^3$. So, substitute the values reached in Eq. (4) into Eq. (3), it is calculated that

$$\begin{aligned} \Delta E_m^3 = -\Delta E_m^1 &= \frac{\left(E_0^3 - E_0^1\right) - \left(\Delta E_f^3 - \Delta E_f^1\right) - (E^3 - E^1)}{2} \\ &= \frac{\left(E_0^3 - E^3\right) - \left(E_0^1 - E^1\right) - \left(\Delta E_f^3 - \Delta E_f^1\right)}{2} \end{aligned} \qquad (5)$$

From Fig. 16, it is seen that the total mechanical energy losses of the No. 1 and No. 3 particles are 9.76 and 8.79 J/kg, respectively. Substituting them into Eq. (5), it can be calculated that the energy exchange between the front and rear parts of the mass induced by momentum transfer is approximately 1.28 J/kg, which occupied about 13.1 and 14.5 % of the total energy losses of the No. 1 and No. 3 particles, respectively.

Taking the example of the No. 1 and No. 3 particles in test No. III, a tentative quantitative analysis of the energy exchange induced by momentum transfer during the avalanche motion is conducted here based on some assumptions and simplifications, hoping to provide some references for the study of the rock avalanche dynamics. From this analysis, it is reached that momentum transfer plays an important role in promoting the travel of the front part of the granular avalanche by delivering the energy of the rear part to the front.
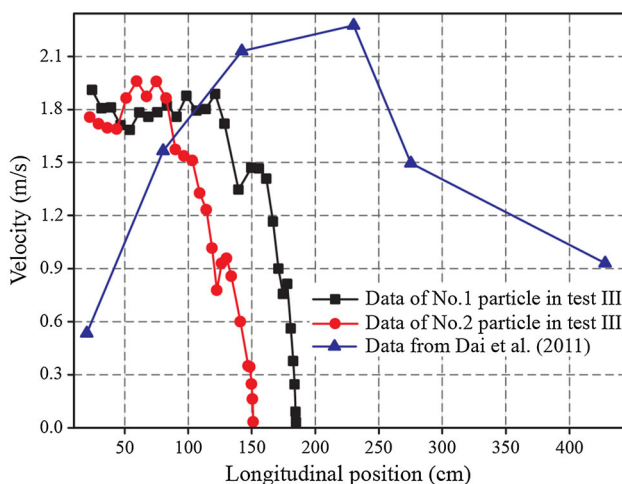
4 Discussion

Aiming to understand the propagation and deposit behaviours of a granular avalanche along a 3D complex basal terrain, a new experimental set-up with natural 3D topography was built here with a series of experiments being conducted. Through these tests, abundant data, including the morphological evolution of the sliding mass, the run-outs and velocities of the surficial particles, the thickness contour and centre of the final deposit, the equivalent frictional coefficient, and the energy dissipation, are documented and analysed. From the preceding presentation of the data, several phenomena revealed in this experimental study of a granular avalanche along a 3D complex basal topography are discussed in the following.

4.1 Comparison Between the Xiejiadianzi Rock Avalanche and the Test Results

Due to the great simplification in the design of the laboratory experiments, some great differences were reached

between the experimental results and natural case, which is important implications for understanding the transport mechanisms of granular flows. Therefore, after the experimental study, a comparison between the Xiejiadianzi rock avalanche and the test results is carried out with two main differences between them being discussed here. The first is the great difference between their run-outs. As revealed in the longitudinal profile of the Xiejiadianzi rock avalanche exhibited in Fig. 1, it can be observed that the failed mass of the Xiejiadianzi rock avalanche is mainly deposited in the lower part of the travelling path, with a fan-shaped morphology presented in plan. The huge volume of the newly formed fan deposits in the lower part seriously blocked the Baishui River with its height of 10–15 m (For detailed information, please refer to Dai et al. 2011). These features are greatly different from the results obtained in this study. As exhibited in Fig. 20 in "Appendix" section, the granular masses of all the tests are mainly accumulated in the upper part of the travelling path with a limited number of particles sporadically accumulated in the lower part. The second great difference is the variations in the velocity curves of the sliding mass. Based on the field investigation, Dai et al. (2011) calculated the velocity variation in the sliding mass along the travelling path of the Xiejiadianzi rock avalanche according to the superelevation and climbing features on the path. For comparison, the velocities calculated by Dai et al. (2011) are mimicked according to the scaling ratio listed in Table 1. And Fig. 18 shows the velocity curves obtained by Dai et al. and this study. It may be observed that the maximum velocity of the Xiejiadianzi rock avalanche is 2.28 m/s, which appears 230.0 cm away from the source area. After the failure of the Xiejiadianzi rock avalanche, the detached mass first experiences an accelerated motion when its horizontal run-

out is less than 230.0 cm. Then, it fails into a deceleration process as the opening of the travelling path. Different from the velocity variation calculated by Dai et al. (2011), the maximum velocity reached in test III is only 1.96 m/s, which distributes at a distance of 59.1 cm away from the source area. And from the velocity variations in the No. 1 and No. 2 particles, it can be seen that there is almost no acceleration process after the failure of the mass in the experimental study.

To explain the great differences between the Xiejiadianzi rock avalanche and this experimental study, the following reasons might play important roles. As aforementioned, the aim of this study was to learn the propagation and deposit characteristics of a granular avalanche along a natural 3D basal terrain and discuss the roles of different factors on the rock avalanche mobility, no attempt is made to reproduce the natural phenomena of the Xiejiadianzi rock avalanche. Hence, in the design of this experimental study, some simplifications were included with the roles of pore fluids and substrate entrainment effect being neglected. This might be one key reason for the occurrence of such great differences. In addition, the volume effect of the experiments might also play a very important role. In real rock avalanches, the volumes usually are $>10^6$ m^3 (Cruden and Varnes 1996) with great thicknesses presented in the vertical direction. And the overburden pressures suffered by the basal facies, the main shearing zone of rock avalanches (Weidinger and Korup 2009), are very high, usually ranging from 1 to 8 MPa (Wang et al. 2015). In the study of the high-velocity shearing tests conducted by Brantut et al. (2008), it was found that when the normal stress suffered by the clay-bearing gouge is over 1 MPa, its residual friction is only about 0.23. And when the normal stress suffered by the clay-bearing gouge is 0.28 MPa, its residual friction can reach 0.5. This indicates that a typical frictional normal stress-weakening can occur during the high-speed motion of rock avalanches. However, as shown in Eq. (1), the role of the frictional normal stress-weakening property of debris was not considered in the design of this study. And it was regarded that the basal friction of debris is constant with different normal stresses and there was no frictional weakening occurred. This simplification is actually different from the feature of natural rock avalanches. Therefore, in this study, the run-outs of the masses are obviously less than that of the Xiejiadianzi rock avalanche.

## 4.2 Geomorphic Control Effect on Avalanche Evolution

Taking the example of test No. III, the morphological evolution of the granular avalanche along the 3D complex basal terrain is introduced in Sect. 3.1. From these

Fig. 18 Comparison of the experimental data and the values calculated by Dai et al.

descriptions, a series of evolved and deposited morphologies, including climbing phenomenon, groove-like trough, and superelevation, are observed. The formation process of the groove-like trough on the surface of the masses indicates that the layout of some local topographies (i.e. small platform in this study) (Figs. 2, 9d) can be a reason for the generation of groove-like trough morphologies on the deposit surface of natural rock avalanches. In addition to the formation of these morphologies along the travelling path, some great differences between the debris travelling along the right and left branch valleys were also observed (Figs. 9d, e, 10, 11), especially with respect to velocity variations. Due to the intensive obstruction of the topography along the left branch valley, a great velocity reduction in the No. 2 particle was observed at a distance of 82.5 cm (Fig. 11) with a higher rate of energy dissipation being revealed as exhibited in Fig. 16 (compared with that of the No. 1 particle). The differences between the debris travelling along both branch valleys further powerfully prove the important of the geomorphic control effect on the avalanche mobility, which can induce a high rate of energy dissipation in the avalanche motion.

4.3 Equivalent Frictional Coefficient of Granular Avalanche

Fahrböschung, defined by the angle of the line connecting the highest point of the starting zone to the tip of the deposited mass, was introduced by Heim (1932) to assess the mobility of a rock avalanche. Considering its disadvantage in the assessment of the rock avalanche mobility (Hsü 1975; Legros 2002), the travel angle of the centre of mass has become more and more popular in the assessment

of avalanche mobility in many physical analyses as the development of monitoring measures (Pudasaini et al. 2005; Cagnoli and Romano 2010; Kokusho and Hiraga 2012; Manzella and Labiouse 2013; Okada and Uchida 2014). In this study, with the help of a three-dimensional laser scanner, the positions of the centres of the avalanche deposits in all tests were computed with their equivalent frictional coefficients being reached as listed in Table 3. It may be observed that the equivalent frictional coefficients of the granular avalanches tested in this study mainly range from 0.48 to 0.57. To further analyse the mobility of a granular avalanche along a 3D complex basal terrain, some results obtained by other researchers are cited in Table 4, and a rough comparison of these results is plotted in Fig. 19.
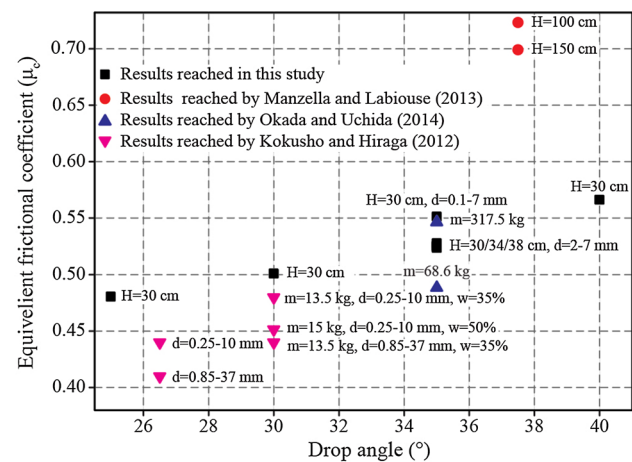
Fig. 19 A rough comparison of the equivalent frictional coefficient reached in this study and by other researchers

Table 4 Test conditions and corresponding results reached by other researchers

Test no.	Set-up form	Test conditions						μ_c	Reference
		Material	Mass, m (kg)	Diameter, d (mm)	Drop angle, α (°)	Drop height, H (cm)	Water content, W (%)		
C1	Inclined chute + horizontal plate	Aquarium gravel	14.3	0.5–4	37.5	150	0	0.70	Manzella and Labiouse
C2			14.3	0.5–4	37.5	100	0	0.72	(2013)
D1	Inclined chute + horizontal plate	Cubic granite	68.6	100	35	230	0	0.49	Okada and Uchida
D2			317.5	100	35	230	0	0.55	(2014)
G-4	Inclined chute	Fluvial gravel	13.5	0.85–37	30	158	35	0.44	Kokusho and Hiraga (2012)
G-5		Fluvial sand	15	0.25–10			50	0.45	
G-6			13.5				35	0.48	
G-12					26.5			0.44	
G-10		Fluvial gravel		0.85–37				0.41	

From Fig. 19, three laws are reached as follows. (1) The comparison of the results obtained in this study and by Manzella and Labiouse (2013) reveals that the equivalent frictional coefficient of a granular avalanche along a 3D topography is obviously lower than that travelling along a set-up composed of an inclined chute and horizontal plate, which indicates that the sharp transition between an inclined chute and horizontal plate can induce a greater reduction in the granular avalanche mobility. (2) The difference between the results reached by Manzella and Labiouse (2013) and Okada and Uchida (2014) reveal that the larger the material grain size, the lower is the energy dissipation, which further proves the validity of the results revealed in this study through the contrast of test Nos. VI and VII. (3) The equivalent frictional coefficient of a granular avalanche travelling along an inclined chute without obstacles, as tested by Kokusho and Hiraga (2012), is the lowest.

Through these comparisons, we can conclude that the effect of a natural 3D topography on the mobility of a granular avalanche is lower than that of a set-up composed of an inclined chute and horizontal plate, and higher than that of a set-up consisting of a single inclined chute. The higher the drop angle and fine particle content, the higher is the equivalent frictional coefficient. The effect of the drop distance on the avalanche mobility is minor. In this study, we primarily analysed the mobility of a granular avalanche along a 3D complex basal terrain using the equivalent frictional coefficient of the mass centre. However, much more research is still needed to learn exactly how the mobility of an avalanche changes when it travels along a 3D complex basal terrain. And the roles of some other factors in natural rock avalanche motion, such as intergranular fluid and substrates entrainment, should also be considered in the future study.

4.4 Improved Representation on Avalanche Mobility

Rock avalanches are extremely rapid granular flows occurred in high mountainous area, which are usually characterized by long run-outs and destructive capacities. Due to its complexity in motion, factors inducing its high mobility along with its dynamical mechanisms are still poorly understood. Research in this field is still continuing, especially in the recent 20 years, with many of physical studies being conducted.

Different from the results reached by other researchers, one major improvement realized in this study is the quantitative analysis of the effect of momentum transfer for avalanche motion. Through the tracing of the four particles distributed on the surface of the sliding mass, we acquired the surficial velocities of the different parts of the sliding mass, which allows us to quantify the energy exchange between the front and rear parts of the sliding mass induced by momentum transfer. In this analysis, it is reached that the energy exchange induced by momentum transfer occupied over 13 % of the total energy losses of the sliding mass, which powerfully confirms that, for a granular avalanche, momentum transfer plays an important effect in the motion of mass, which can greatly accelerate the velocity of particles in the front part through delivering the kinetic energy of the rear part to the front. This result is reached on some assumptions and simplification, so further study is still needed in the future to exactly quantify the effect of momentum transfer.

5 Conclusions

To understand how a rock avalanche propagates across a natural 3D complex basal topography, a series of tests are designed in this study with the geomorphic control effect, material grain size effect, drop angle effect, and drop distance effect on rock avalanche mobility being analysed. From the analysis of these parameters, some interesting conclusions enabling a better understanding of rock avalanches are reached.

1. Under the control of the topography along the travelling path, the propagation process of the granular avalanche can be divided into three stages, i.e. the initial failure stage, diverted flow stage, and movement stage after convergence.
2. Through a comparison of the evolutions of the debris along the right and left branch valleys, an obvious geomorphic control effect on avalanche mobility is revealed, i.e. the higher the complexity of topography along the travelling path, the higher the energy dissipation rate.
3. For the granular avalanche tested in this study, the equivalent frictional coefficients of the granular avalanches range from 0.48 to 0.57, which is lower than that reached with a set-up composed of an inclined chute and horizontal plate and higher than that reached using a set-up composed of an inclined chute only. And the higher the drop angle and fine particle content, the higher the equivalent frictional coefficient. The effect of the drop distance on the avalanche mobility is minor.
4. For granular avalanches, momentum transfer has an important effect on the motion of mass, which can accelerate the mobility of the front part greatly through delivering the kinetic energy of the rear part to the front. In this experiment, a tentative quantitative analysis reveals that the energy exchange induced by

momentum transfer occupied over 13 % of the total energy loss of the sliding mass.

5. In the motion of the granular avalanche, some interesting features, such as groove-like trough and superelevation, are observed under the control of certain topographies, which indicates that the topographic interference controls the propagation form of the mass in a great degree.

Appendix

Part I

In order to provide more information on the propagation and deposit features of granular avalanche along a natural 3D topographical terrain, some results of other tests are supplemented in this part.

See Figs. 20, 21, 22 and Table 5.
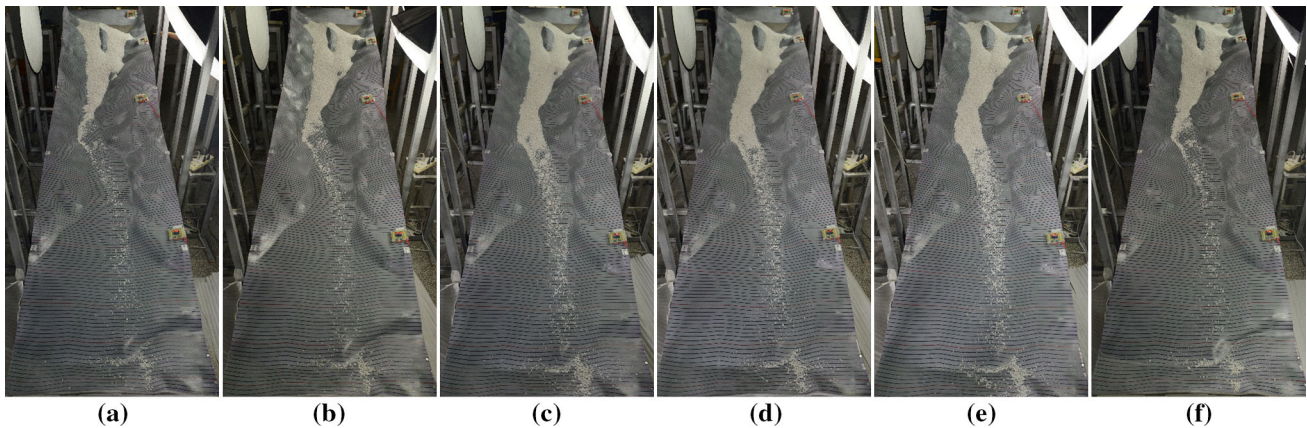
Fig. 20 Final deposit of the rest tests to show the main accumulated areas of the granular avalanches. **a** Test No. I, **b** test No. II, **c** test No. IV, **d** test No. V, **e** test No. VI, **f** test No. VII
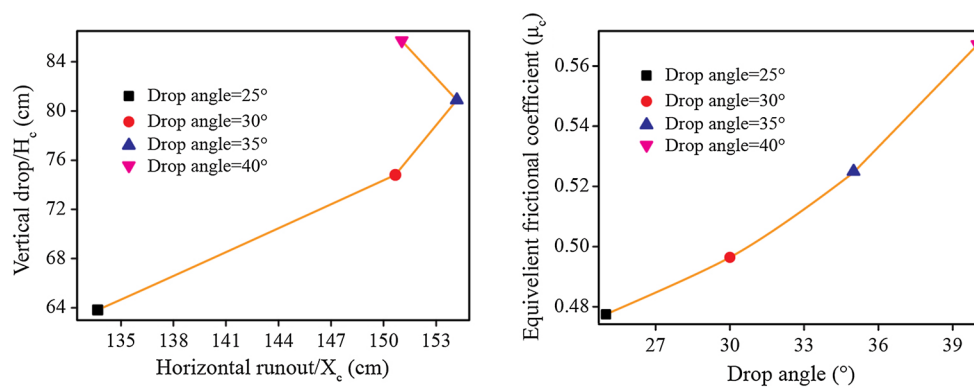
Fig. 21 Support materials for the conclusions reached from Fig. 15a

Fig. 22 Support materials for the conclusions reached from Fig. 15b
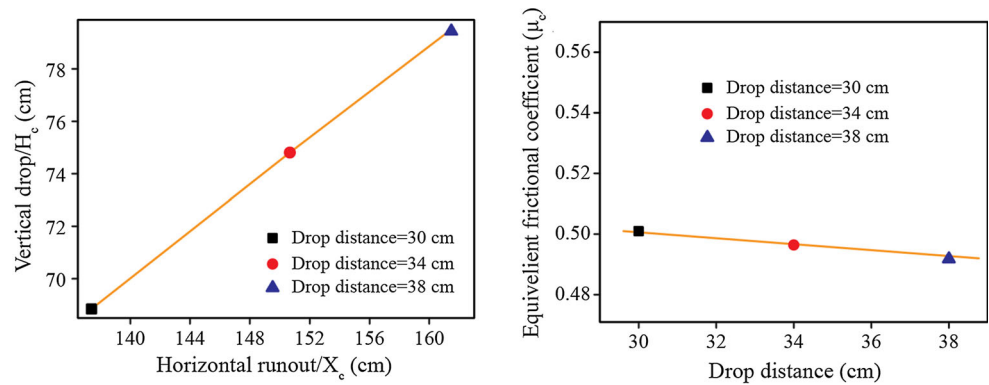

**Table 5** Parallel test conditions and corresponding tested data of mass centre

Test no.	Material	Test conditions					Tested data of mass centre		
		Mass (kg)	Basal friction	Diameter (mm)	Drop angle (°)	Drop distance (cm)	X_c (cm)	H_c (cm)	μ_c
1	Quartz gravel	17.6	Nearly smooth	2–7	25	34	133.7	63.8	0.478
2					30	34	150.7	74.8	0.496
3					40	34	151.0	85.6	0.567
4					30	38	161.5	79.5	0.492

Part II

Calculation of the bulk mechanical energy variations in the No. 1 and No. 3 particles shown in Fig. 16.

As mentioned in this paper, three digital video cameras were used to record videos of the propagation of the granular avalanche, which allows us to obtain the data on the run-outs and velocities of the No. 1 and No. 3 particles (Fig. 11). In addition, a three-dimensional laser scanner was employed to acquire the final deposit of the granular avalanche. According to the positions of the particles

recorded by cameras at any moment (Fig. 23a), we projected their positions on the map obtained using the three-dimensional laser scanner (Fig. 23b) and calculated their vertical drops. With this method, the vertical drops of the No. 1 and No. 3 particles at any moment we reached are listed in Table 6. Here, considering that the thickness of the debris at any moment is greatly smaller than the vertical drops of the No. 1 and No. 3 particles, so we neglected it in the calculation of the particles' drops. With the data listed in Table 6 and the velocity variations in the particles exhibited in Fig. 11, the bulk mechanical energy variations
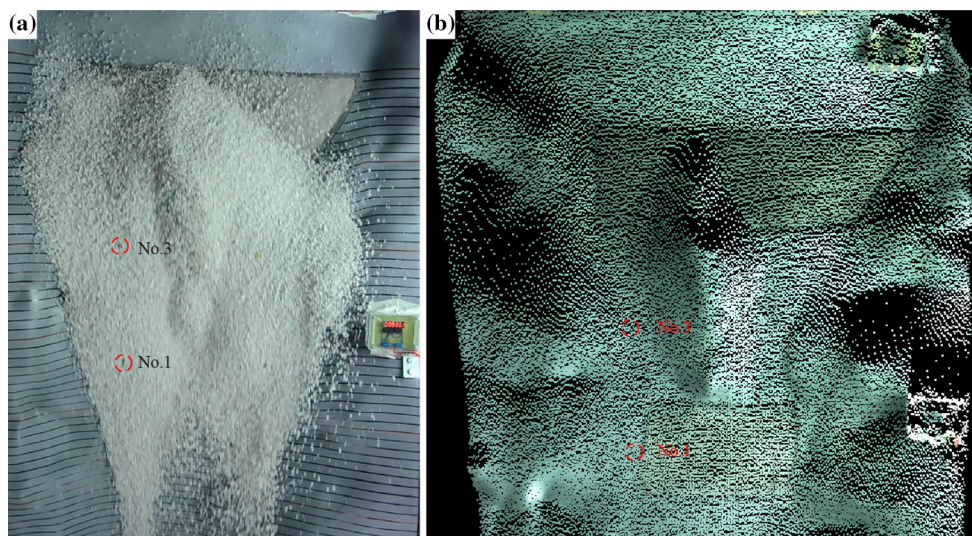
Fig. 23 Introduction for the calculation of particles' vertical drops at any moment (**a** photograph recorded by camera, **b** scanned data)

Table 6 Data of the vertical drops of the No. 1 and No. 3 particles at any moment

No. 1			No. 3		
Horizontal run-out (cm)	Vertical drops (cm)	Bulk mechanical energy (J/kg)	Horizontal run-out (cm)	Vertical drops (cm)	Bulk mechanical energy (J/kg)
−45	0	2.88	−68	0	4.17
10.15	6.71	1.27	7.85	5.426	1.70
24.13	13.32	0.53	19.32	11.496	0.36
31.58	16.22	0.05	26.22	14.156	−0.22
39.01	18.70	−0.18	32.66	16.576	−0.54
46.51	21.81	−0.66	38.79	18.806	−0.84
53.83	23.57	−0.88	44.38	20.926	−1.19
61.21	26.85	−1.03	49.5	22.666	−1.44
68.48	29.68	−1.35	54.49	24.306	−1.67
75.57	32.36	−1.57	59.41	26.176	−1.92
82.97	35.17	−1.78	64.17	27.971	−2.15
90.58	37.72	−2.14	68.87	29.956	−2.29
98.4	40.70	−2.22	73.54	31.806	−2.45
106.21	43.63	−2.66	78.02	33.346	−2.67
113.59	45.95	−2.87	82.32	35.173	−2.93
120.98	48.84	−2.99	88.31	37.24	−3.24
128.38	52.11	−3.62	93.92	39.21	−3.50
139.29	56.32	−4.61	97.28	40.35	−3.62
149.53	59.65	−4.76	100.70	41.49	−3.70
155.42	61.42	−4.94	103.91	42.44	−3.94
161.18	63.54	−5.23	106.54	43.47	−4.10
166.45	65.72	−5.75	108.78	44.34	−4.23
170.83	66.79	−6.14	110.58	44.79	−4.31
174.38	67.63	−6.34	112.13	45.41	−4.38
177.67	68.56	−6.38	113.35	45.82	−4.47
180.44	69.01	−6.60	114.1	46.10	−4.51
182.30	69.62	−6.75	114.72	46.47	−4.54
183.58	69.96	−6.82	115.34	46.65	−4.56
184.30	70.18	−6.87	115.82	46.81	−4.58
184.58	70.21	−6.879	116.18	47.03	−4.60
184.66	70.22	−6.88	116.36	47.11	−4.62

The leading edge of source area is the zero point of run-out and the zero potential level

in the No. 1 and No. 3 particles were reached as shown in Fig. 16.

References

Bagnold RA (1954) Experiments on gravity-free dispersion of large solid sphere in a Newtonian fluid under shear. Proc R Soc 225(1160):49–63

Bartali R, Sarocchi D, Nahmad-Molinari Y (2015) Stick-slip motion and high speed ejecta in granular avalanches detected through a multi-sensors flume. Eng Geol 195:248–257

Boultbee N, Stead D, Schwab J et al (2006) The Zymoetz River rock avalanche, June 2002, British Columbia, Canada. Eng Geol 83(1–3):76–93

Brantut N, Schubnel A, Rouzaud JN et al (2008) High-velocity frictional properties of a clay-bearing fault gouge and implications for earthquake mechanics. J Geophys Res 113(B10401):1–18

Bryant SK, Take WA, Bowman ET (2015a) Observations of grain-scale interactions and simulation of dry granular flows in a large-scale flume. Can Geotech J 52(5):638–655

Bryant SK, Take WA, Bowman ET et al (2015b) Physical and numerical modelling of dry granular flows under Coriolis conditions. Géotechnique 65(3):188–200

Cagnoli B, Piersanti A (2015) Grain size and flow volume effects on granular flow mobility in numerical simulations: 3-D discrete element modeling of flows of angular rock fragments. J Geophys Res 120(4):2350–2366

Cagnoli B, Romano GP (2010) Pressures at the base of dry flows of angular rock fragments as a function of grain size and flow volume: experimental results. J Volcanol Geoth Res 196(3–4):236–244

Cagnoli B, Romano GP (2012) Granular pressure at the base of dry flows of angular rock fragments as a function of grain size and flow volume: a relationship from laboratory experiments. J Geophys Res 117(B10):1–12

Choi CE, Au-Yeung SCH, Ng CWW et al (2015) Flume investigation of landslide granular debris and water runup mechanisms. Géotech Lett 5:28–32

Cox SC, Allen SK (2009) Vampire rock avalanches of January 2008 and 2003, Southern Alps, New Zealand. Landslides 6(2):161–166

Cruden DM, Lu ZY (1992) The rockslide and debris flow from Mount Cayley, B.C., in June 1984. Can Geotech J 29(4):614–626

Cruden DM, Varnes DJ (1996) Landslide types and processes. In: Turner AK, Schuster RL (eds) Landslides-investigation and mitigation. National Academy Press, Washington, pp 36–75

Dai FC, Tu XB, Xu C et al (2011) Rock avalanches triggered by oblique-thrusting during the 12 May 2008 Ms 8.0 Wenchuan earthquake, China. Geomorphology 132(3–4):300–318

Davies TRH (1982) Spreading of rock avalanche debris by mechanical fluidization. Rock Mech 15(1):9–24

Davies TRH, McSaveney MJ, Hodgson KA (1999) A fragmentation-spreading model for long-runout rock avalanches. Can Geotech J 36(6):1096–1110

Deline P, Alberto W, Broccolato M et al (2011) The December 2008 Crammont rock avalanche, Mont Blanc massif area, Italy. Nat Hazards Earth Syst Sci 11(12):3307–3318

Drake TG (1991) Granular flow: physical experiments and their implications for microstructural theories. J Fluid Mech 225:121–152

Dufresne A (2012) Granular flow experiments on the interaction with stationary runout path materials and comparison to rock avalanche events. Earth Surf Proc Land 37(14):1527–1541

Dufresne A, Davies TR (2009) Longitudinal ridges in mass movement deposits. Geomorphology 105(3–4):171–181

Evans SG (1989) Rock avalanche run-up record. Nature 340(6231):271

Félix G, Thomas N (2004) Relation between dry granular flow regimes and morphology of deposits: formation of levees in pyroclastic deposits. Earth Planet Sci Lett 221(1–4):197–213

Friedmann SJ, Taberlet N, Losert W (2006) Rock-avalanche dynamics: insights from granular physics experiments. Int J Earth Sci 95(5):911–919

George DL, Iverson RM (2014) A depth-averaged debris-flow model that includes the effects of evolving dilatancy. II. Numerical predictions and experimental tests. Proc R Soc A 470(2170):1–31

Habib P (1975) Production of gaseous pore pressure during rock slides. Rock Mech 7(4):193–197

Hadley JB (1978) Madison Canyon rockslide, Montana, U.S.A. In: Voight B (ed) Rockslides and avalanches. Elsevier, Amsterdam, pp 167–180

Heim A (1932) Landslides and human lives. Bitech Publishers, Vancouver, pp 93–94

Hsü KJ (1975) Catastrophic debris streams (sturzstroms) generated by rockfalls. Bull Geol Soc Am 86(1):225–256

Hutter K, Koch T (1991) Motion of a granular avalanche in an exponentially curved chute: experiments and theoretical predictions. Philos Trans R Soc Lond Ser A 334(1633):93–138

Iverson RM (2015) Scaling and design of landslide and debris-flow experiments. Geomorphology 244:9–20

Iverson RM, Logan M, Denlinger RP (2004) Granular avalanches across irregular three-dimensional terrain: 2. Experimental tests. J Geophys Res 109(F1):1–11

Iverson RM, Logan M, LaHusen RG et al (2010a) The perfect debris flow? Aggregated results from 28 large-scale experiments. J Geophys Res 115(F3):1–29

Iverson RM, Reid ME, Logan M et al (2010b) Positive feedback and momentum growth during debris-flow entrainment of wet bed sediment. Nat Geosci 4(2):116–121

Jiang YJ, Towhata I (2013) Experimental study of dry granular flow and impact behavior against a rigid retaining wall. Rock Mech Rock Eng 46(4):713–729

Johnson CG, Kokelaar BP, Iverson RM et al (2012) Grain-size segregation and levee formation in geophysical mass flows. J Geophys Res 117(F01032):1–23

Keefer DK, Larsen MC (2007) Assessing landslide hazards. Science 316(5828):1136–1138

Kent PE (1966) The transport mechanism in catastrophic rock falls. J Geol 74(1):79–83

Kobayashi Y (1994) Effect on basal guided waves on landslides. Pure Appl Geophys 142(2):329–346

Kokelaar BP, Graham RL, Gray JMNT et al (2014) Fine-grained linings of leveed channels facilitate runout of granular flows. Earth Planet Sci Lett 385:172–180

Kokusho T, Hiraga Y (2012) Dissipated energies and friction coefficients in granular flow by flume tests. Soils Found 52(2):356–367

Legros F (2002) The mobility of long-runout landslides. Eng Geol 63(3):301–331

Longchamp C, Abellan A, Jaboyedoff M et al (2015) 3-D models and structural analysis of analogue rock avalanche deposits: a kinematic analysis of the propagation mechanism. Earth Surf Dyn Discuss 3(4):1255–1288

Mancarella D, Hungr O (2010) Analysis of run-up of granular avalanches against steep, adverse slopes and protective barriers. Can Geotech J 47(8):827–841

Mangeney A, Roche O, Hungr O et al (2010) Erosion and mobility in granular collapse over sloping beds. J Geophys Res 115(F3):1–23

Manzella I, Labiouse V (2008) Qualitative analysis of rock avalanches propagation by means of physical modelling of non-constrained gravel flows. Rock Mech Rock Eng 41(1):133–151

Manzella I, Labiouse V (2009) Flow experiments with gravel and blocks at small scale to investigate parameters and mechanisms involved in rock avalanches. Eng Geol 109(1–2):146–158

Manzella I, Labiouse V (2013) Empirical and analytical analyses of laboratory granular flows to investigate rock avalanche propagation. Landslides 10(1):23–36

McDougall S, Hungr O (2004) A model for the analysis of rapid landslide motion across three dimensional terrain. Can Geotech J 41(6):1084–1097

Melosh HJ (1986) The physics of very large landslides. Acta Mech 64(1–2):89–99

Nicoletti PG, Sorriso-Valvo M (1991) Geomorphic controls of the shape and mobility of rock avalanches. Geol Soc Am Bull 103(10):1365–1373

Okada Y, Uchida I (2014) Dependence of runout distance on the number of rock blocks in large-scale rock-mass failure experiments. J For Res 19(3):329–339

Okura Y, Kitahara H, Sammori T (2000) Fluidization in dry landslides. Eng Geol 56(3):347–360

Ostermann M, Sanders D, Ivy-Ochs S et al (2012) Early Holocene (8.6 ka) rock avalanche deposits, Obernberg valley (Eastern Alps): landform interpretation and kinematics of rapid mass movement. Geomorphology 171–172:83–93

Paguican EM, Vries BVWD, Lagmay A (2014) Hummocks: how they form and how they evolve in rockslide-debris avalanches. Landslides 11(1):67–80

Pouliquen O (1999) Scaling laws in granular flows down rough inclined planes. Phys Fluids 11(3):542–548

Preuth T, Bartelt P, Korup O, McArdell BW (2010) A random kinetic energy model for rock avalanches: eight case studies. J Geophys Res 115:F03036. doi:10.1029/2009JF001640

Pudasaini SP, Miller SA (2013) The hypermobility of huge landslides and avalanches. Eng Geol 157:124–132

Pudasaini SP, Hsiau SS, Wang YQ et al (2005) Velocity measurements in dry granular avalanches using particle image velocimetry technique and comparison with theoretical predictions. Phys Fluids 17(9):1–10

Pudasaini SP, Wang YQ, Sheng LT et al (2008) Avalanching granular flows down curved and twisted channels: theoretical and experimental results. Phys Fluids 20(7):073302–073312

Scheidl C, McArdell BW, Rickenmann R (2015) Debris-flow velocities and superelevation in a curved laboratory channel. Can Geotech J 52(3):305–317

Shea T, Vries BVWD (2008) Structural analysis and analogue modeling of the kinematics and dynamics of rockslide avalanches. Geosphere 4(4):657–686

Shreve RL (1968) Leakage and fluidization in air-lubricated avalanches. Geol Soc Am Bull 79(5):653–658

Turnbull B, Bowman ET, McElwaine JN (2015) Debris flows: experiments and modelling. C R Phys 16:86–96

Wang FW, Cheng QG, Highland L et al (2009) Preliminary investigation of some large landslides triggered by the 2008 Wenchuan earthquake, Sichuan Province, China. Landslides 6(1):47–54

Wang YF, Cheng QG, Zhu Q (2012) Inverse grading analysis of deposit from rock avalanches triggered by Wenchuan earthquake. Chin J Rock Mech Eng 31(6):1089–1106 **(in Chinese)**

Wang GH, Huang RQ, Chigira M et al (2013) Landslide amplification by liquefaction of runout-path material after the 2008 Wenchuan (M 8.0) earthquake, China. Earth Surf Proc Land 38(3):265–274

Wang YF, Cheng QG, Zhu Q (2015) Surface microscopic examinations of quartz grains from rock avalanche basal travel zones. Can Geotech J 52(2):167–181

Weidinger JT, Korup O (2009) Frictionite as evidence for a large Late Quaternary rockslide near Kanchenjunga, Sikkim Himalayas, India—implications for extreme events in mountain relief destruction. Geomorphology 103(1):57–65

Xu Q, Shang YJ, Asch TV et al (2012) Observations from the large, rapid Yigong rock slide-debris avalanche, southeast Tibet. Can Geotech J 49(5):589–606

Yang QQ, Cai F, Ugai K et al (2011) Some factors affecting the frontal velocity of rapid dry granular flows in a large flume. Eng Geol 122(3–4):249–260

Yin YP, Sun P, Zhang M et al (2011) Mechanism on apparent dip sliding of oblique inclined bedding rockslide at Jiweishan, Chongqing, China. Landslides 8(1):49–65

Zhang M, Yin YP (2013) Dynamics, mobility-controlling factors and transport mechanisms of rapid long-runout rock avalanches in China. Eng Geol 167:37–58